Chemomechanical properties of antiwear films using X-ray absorption microscopy and nanoindentation techniques

Mark A. Nicholls[a], G. Michael Bancroft[a], Peter R. Norton[a,*], Masoud Kasrai[a], Gelsomina De Stasio[b], Bradley H. Frazer[b] and Lisa M. Wiese[c]

[a]*Department of Chemistry, University of Western Ontario, London, Ontario, Canada N6A 2B7*
[b]*Department of Physics, University of Wisconsin-Madison, Madison, WI 53706-1390, USA*
[c]*Syncrotron Radiation Center, University of Wisconsin-Madison, Stoughton, WI 53589, USA*

Received 3 November 2003; accepted 22 December 2003

The first chemomechanical comparison between an antiwear film formed from a solution containing zinc dialkyl-dithiophosphates (ZDDPs) to a solution containing ZDDP plus a detergent (ZDDPdet) has been performed. X-ray absorption near-edge structure (XANES) analysis has shown a difference in the type of polyphosphate between each film. The ZDDPdet film has been found to contain short-chain polyphosphates throughout. X-ray photoelectron emission microscopy (X-PEEM) has provided detailed spatially resolved microchemistry of the films. The large pads in the ZDDP antiwear film have long-chain polyphosphates at the surface and shorter-chain polyphosphates are found in the lower lying regions. The spatially resolved chemistry of the ZDDPdet film was found to be short-chain calcium phosphate throughout. Fiducial marks allowed for the re-location of the same areas with an imaging nanoindenter. This allowed the nanoscale mechanical properties, of selected antiwear pads, to be measured on the same length scale. The indentation modulus of the ZDDP antiwear pads were found to be heterogeneous, ~120 GPa at the center and ~90 GPa at the edges. The ZDDPdet antiwear pads were found to be more uniform and have a similar indentation modulus of ~90 GPa. A theory explaining this measured difference, which is based on the probing depths of all techniques used, sheds new insight into the structure and mechanical response of ZDDP antiwear films.

KEY WORDS: nanotribology, XANES spectroscopy, ZDDP, detergents, X-ray spectromicroscopy, mechanical properties, nanoindentation

1. Introduction

Understanding the mechanism by which zincdialkyldithiophosphates (ZDDPs) minimize asperity contact and hence reduce wear, is becoming more imperative as environmental concerns begin to push for the reduction of ZDDP contained in engine oils. ZDDPs have long been added for their antioxidant, antiwear and extreme pressure wear protection. ZDDPs have been studied on the chemical level for many decades and only recently the apparent mechanism by which they minimize wear has been partially understood. It is widely accepted that ZDDPs breakdown in the unforgiving conditions in a combustion engine to create reaction products that, under high temperature and pressure, create sacrificial films that are responsible for minimizing asperity contact [1]. The exact mechanism by which ZDDP decomposes is still under debate. However, recent studies using X-ray absorption spectroscopy (XAS) have shown that thiophosphates and phosphates are created by decomposition of the ZDDP at the metallic surface. This interaction is responsible for forming a polyphosphate film [2–5]. X-ray absorption near-edge structure (XANES) spectroscopy has shown that the film is composed of a bilayer structure in which short-chain polyphosphates are located at the substrate (metal)/film interface and longer-chain polyphosphates are located at the near-surface region [2,6,7]. The cations such as zinc and iron are network modifiers for the polyphosphate glass structure. The multi-valent cations, have been suggested as being responsible for cross-linking the polyphosphate groups and forming the long-chain and possibly metaphosphate structures [7].

Due to the difficulties of studying films in situ, the vast majority of surface morphology and topography determination has been done after the rubbing process has been stopped. Scanning electron microscopy (SEM) [8–11] and atomic force microscopy (AFM) [12–14] have provided morphological and topographical information about the films. It is well accepted that the films have a mottled appearance across the rubbing surfaces. The mottled nature of the film is representative of the rubbing history. Close examination of the mottled structure shows the agglomeration of patches

*To whom correspondence should be addressed.
E-mail: pnorton@uwo.ca

1023-8883/04/0800–0245/0

of small and large features that are raised from the surface. These features, termed antiwear pads, can be on the order of 300 nm in height [12–14]. Extensive topographic imaging has shown that the antiwear pads are elongated in the direction of rubbing [13,15] and that the pads are located in regions that conform to the contacting points on the reciprocating counter-surface [13]. Recent studies of the antiwear pads, using nanoindentation techniques, have shown that the pads have unique elastic and viscoelastic properties. There have been two main regions identified by topographic imaging: regions containing the large (and or) small antiwear pads and regions between these pads (valleys). It has also been determined that the films are, mechanically, extremely heterogeneous. The antiwear pads have been found to have an indentation modulus (E_s^*) between 70 and 150 GPa [12–14,16,17] and regions between the pads have been found to be much softer and more susceptible to plastic deformation, with an E_s^* of ~35 GPa [12,13]. A detailed study of the antiwear pads using an interfacial force microscope (IFM) [18–20] has shown heterogeneity along and across the pads [12,14]. It has been found that the centre of the pads are much stiffer and more elastic than at the edges of the pads. This difference is probably due to the higher loads experienced at the centre of the pads due to the load applied by the counter-surface causing a transformation of the material properties [12].

Advancements in the area of nanotechnology have demanded an improvement in the spatial resolution of many surface analytical techniques. One such improvement is in XANES imaging, using an X-ray photoelectron emission microscope (X-PEEM) [21–23]. It is now possible to obtain spatially resolved XANES analysis of sub-100 nm areas. This has now allowed for the spatially resolved chemical analysis of ZDDP antiwear films [7,24]. In combination with nanoindentation, the first ever chemomechanical characterization of ZDDP antiwear films were performed [7]. X-PEEM analysis with a pixel resolution of ~200 nm and nanoindentation measurements at approximately the same length-scale, were performed on ZDDP antiwear pads. It was found that the surfaces of the large antiwear pads were composed of longer-chain polyphosphates and regions between the pads were a mixture of shorter-chain polyphosphates and some unreacted ZDDP. The E_s^* calculated for the large antiwear pads was found to be ~81 GPa in agreement with others [12–14,16].

Fully formulated engine oil contains varying concentrations of detergents, dispersants, emulsifiers, viscosity improvers, antiwear and antioxidant additives to name only a few. This greatly complicates the chemical reactions that are occurring in the engine oil and at the rubbing surfaces, many of which can have anti-synergistic effects. Important additives are detergents and dispersants that are responsible for keeping insoluble products in suspension so that they can be removed by filters. Concentrations of detergents can vary from one engine oil formulation to the next, but generally make-up about 5% of the oil formulation [25]. Many detergents are metallic sulphonates, salicylates and phenates [25]. Detergents have neutral and basic forms; some are also available in overbased forms. An overbased additive is one in which $CaCO_3$ is incorporated into the organic structure to provide a reservoir of alkalinity. The total base number (TBN) is a measure of alkalinity and is defined as the amount (mg) of KOH required, per gram of additive. It has been found that metallic detergents have a anti-synergistic effect on ZDDP inhibiting its ability as an antiwear agent [11,26–30]. XANES analysis has shown that metallic overbased detergents affect ZDDP decomposition and results in the formation of a short-chain polyphosphate antiwear films [27,29,31]. It was determined that the film lacked the bilayer structure (long-chain at the surface, shorter-chain in the bulk) that solutions containing ZDDP alone form. In contrast, the ZDDP plus detergent film was composed of *uniform* shorter-chain polyphosphates throughout. The authors suggest [27] that the poorer antiwear protection is due to the elimination of the long-chain polyphosphate film and the formation of shorter-chain calcium phosphate.

In this study, detailed chemomechanical mapping, at high resolution, has been attempted to provide a comprehensive evaluation of the ZDDP antiwear film generated in the presence of an overbased metallic detergent. The chemical and mechanical properties of selected features in the film have been compared to those of an antiwear film formed from ZDDP in base oil alone. This is the first investigation into the nanomechanical response of a long- and shorter-chain polyphosphate film with the intention of understanding why one is a better antiwear film than the other. This will provide a unique perspective into understanding why ZDDP antiwear films are so effective and what exclusive characteristics are required to create ideal antiwear films.

2. Experimental

2.1. Antiwear film formation

The ZDDP antiwear films were formed in a Plint wear tester under fullyflooded, boundary lubrication conditions. The test geometry was a cylinder-on-flat establishing a sliding line contact. The reciprocating cylinder was manufactured from low alloy 52100 steel 6 mm in diameter and 6 mm in length. The steel samples were also manufactured from 52100 steel into square specimens 10 mm × 10 mm × 4 mm in thickness. The steel samples (coupon) and pins were austenitized and quenched. Their hardness was >60

Rockwell C. The coupons were polished with 3 μm diamond paste to a surface roughness of ~10 nm determined by atomic force microscopy. The test conditions consisted of a rubbing time of 1 h at 100 °C, with an applied load of 220 N and a frequency of 25 Hz. The ZDDP solution was a commercial ZDDP obtained in pre-concentrated form from Imperial Oil, Canada. The commercial concentrate is a mixture of neutral and basic forms, consisting of secondary butyl (85%) and *n*-octyl (15%) groups. The concentrate was diluted using MCT-10 base oil to 1.2 wt.% resulting in a phosphorus content of ~0.1% by weight. MCT-10 base oil is a mineral oil with a maximum sulfur content of 0.25 mass percent. An identical solution containing 1.2 wt.% ZDDP plus 2 wt.% overbased calcium sulphonate (TBN 400) in MCT-10 base oil was prepared. The films were washed with hexanes before analysis. A grid composed of fiducial marks was created using a Vickers hardness tester using loads of 100 and 500 g which made indents ~25 and ~150 μm across, respectively. This grid allowed for re-location of the same regions with the multiple techniques discussed below.

2.2. XANES and X-PEEM analysis

Phosphorus and sulfur K- and L-edge X-ray absorption spectra give detailed information about the local environment and oxidation of phosphorus and sulfur in a film or on a surface. There are two modes of analysis offered by XANES that have different sensitivities providing a thorough characterization of the surface and bulk properties of the films. At the P K-edge, the fluorescence yield (FY) mode of detection is a bulk technique and can probe >800 nm of a film, while the total electron yield (TEY) mode probes ~50 nm [32]. At the P L-edge, the detection limits for the FY mode is ~60 nm and ~5 nm for the TEY mode. The phosphorus L- and K-edges data were collected at the 1 GeV Aladdin storage ring, University of Wisconsin, Madison, WI. The K-edge data were recorded using the double-crystal monochromator (DCM) beamline with a photon resolution of ~0.9 eV and the L-edge data were obtained using the Grasshopper beamline with a ~0.1 eV photon resolution. Details of the TEY and FY measurements are given elsewhere [33]. Similar resolution is obtained at the sulfur K- and L-edges. Two individual scans were recorded for each specimen and digitally combined. The spectra were normalized against I_o and a linear background was then removed.

X-PEEM was performed using the SPHINX [34] microscope (ELMITEC GmbH) installed on the 6 m-TGM (Toroidal Grating Monochromator) beamline at the 1 GeV Aladdin storage ring, University of Wisconsin, Madison, WI (for details see Ref. [7,35]. The high-energy grating was optimized to give ~0.1 eV resolution at the P L-edge. Image intensity in X-PEEM is similar to the XANES TEY and surface sensitivity of the instrument was limited by the escape depth of the secondary electrons at the P L-edge (~2–5 nm) [32,35]. However, there are many other contributions to the signal generation process—topography, shadowing, charging, variable sampling depth and work function, among others. Thus one of the challenges of this work was to develop and use analysis techniques which emphasized the chemical (X-ray absorption) information while simultaneously de-emphasize the other contrast factors. Spatial distribution, in the SPHNIX microscope is maintained by the use of a large electric field (20 keV) between the sample and the aperture. The resolution obtained in the images was chosen to be ~200 nm per pixel. Sequences of images (0.1–0.2 eV step size) were combined to produce a three-dimensional data set or spectromicroscopy 'stack' [21] that was analyzed to extract detailed phosphorus and sulfur information about the antiwear films using aXis200 software [36]. After the first X-PEEM images and nanoindentation tests were performed the sample was then sputter coated with 10 Å of platinum and imaged again with the SPHNIX spectromicroscope. The 10 Å platinum coating is used to reduce the charging of the thick antiwear films [37,38].

2.3. Nanomechanical property testing

The surfaces were extensively examined prior to X-PEEM analysis using a NanoScope IIIa® atomic force microscope (AFM) from Digital Instruments (Santa Barbara, CA, USA). Topographic images allowed for detailed understanding of the morphology and selection of features of interest. The nanomechanical properties of the antiwear films were examined using a force transducer® from Hysitron Inc (Minneapolis, MN, USA). The transducer was mounted on an AFM-1 base, which then allows for simultaneous constant force imaging using the same tip as used for the indentation procedure. The tip is a Berkovich diamond with a radius of curvature of 100–160 nm. This allows for topographic images to be taken, with a sub −0.5 μm resolution and selection of specific features to perform mechanical property tests. The tandem system allows for accurate measurement of the displacement of the tip during the indentation process. The acquisition of force–displacement (f–d) curves allow for the calculation of the hardness and reduced elastic moduli (E^*) using the initial slope of the unloading curve as suggested by Oliver and Pharr [39]. The system was calibrated for compliance and tip abnormalities, using the commonly accepted method of measuring a succession of indents into fused silica at different penetration depths to calculate the tip area function [40,41]. The reduced elastic modulus is defined through the equation

$$\frac{1}{E^*} = \frac{\left(1 - v_s^2\right)}{E_s} + \frac{\left(1 - v_i^2\right)}{E_i} \quad (1)$$

where E_s and v_s are the Young's modulus and Poisson's ratio of the sample, respectively and E_i and v_i are the respective values for the indenter. The values listed in this report are the indentation modulus of the sample E_s*, given by

$$E_s^* = \frac{E_s}{\left(1 - v_s^2\right)} = \left[\frac{1}{E^*} - \left(\frac{1 - v_i^2}{E_i}\right)\right]^{-1} \quad (2)$$

in which the tip properties have been removed from the reduced modulus value ($E_i = 1140$ GPa; $v_i = 0.07$) in Eq. (1). Selected antiwear pads and other features of interest, were chosen to perform indentation tests. The antiwear pads were chosen because they were identified in the X-PEEM images and thus analysed chemically. The fiducial marks applied to the surface allowed for the re-location of the same areas with all techniques. The soft X-rays used during the XANES acquirement of data had no apparent affect of modifying the film and thus accurate measurement of the mechanical properties could still be performed. From topography images taken with the AFM and the imaging nanoindenter, the approximate film thickness was known and care was taken to use maximum loads that kept the penetration depth into the film under 10% of film thickness. This minimized the possibility of forming pile-up and exceeding the 10% rule-of-thumb for measuring mechanical properties of soft films on a rigid substrate [40,42,43]. Topographic images were taken before and after indents using the same tip. Successions of indents were performed along or across the selected features and the indentation moduli of the films were calculated. Indents were spaced >300 nm apart to avoid any affects of plastic deformation or alteration of the film from adjacent indents.

3. Results and discussion

3.1. Macro analysis at the phosphorus L-edge, XANES

Phosphorus L-edge spectroscopy provides detailed oxidation and local geometry information about the P species present in the ZDDP antiwear films. This is possible due to the narrow line widths and high photon resolution at the L-edge. L-edge spectroscopy probes the excitation of electrons from P2p occupied orbitals to unoccupied antibonding orbitals. Model compounds, with known composition, are used as reference materials to identify the P species present in the film. The large area spectra are obtained from an X-ray spot size ($\sim 2 \times 3$ mm^2) and give an overall average spectrum for the antiwear film. In figure 1, spectra for model compounds zinc polyphosphate and calcium orthophosphate are shown along with the spectrum for unreacted ZDDP. The characteristic triplet observed for ZDDP can be observed [2]. The spectra of the zinc and calcium phosphates are shifted to higher energy and these spectra show four peaks *a*, *b*, *c* and *d*. The peaks for the calcium orthophosphate are shifted to lower energy by ~0.5 eV compared to the zinc polyphosphate spectrum and a broad shoulder s_1 is also apparent which is not present in the zinc polyphosphate spectrum. Different electronegativities for the two cations result in slightly different antibonding orbital mixing.

It has been determined from previous work [2,4–6, 14,44] that ZDDP antiwear films have a polyphosphate structure similar to that for the zinc polyphosphate glass (e.g., $Zn_6P_{10}O_{31}$). In figure 1, the total electron yield (TEY) spectrum from the ZDDP antiwear film shows peaks *a*, *b* and *c* shifted to higher energy from peaks 1, 2 and 3 of unreacted ZDDP thus indicating decomposition of ZDDP has occurred and a zinc polyphosphate has been formed. The assignments for peaks *a–d* have been made elsewhere [45,46]. The TEY spectra, at the P L-edge, probe the topmost surface (~5 nm) [32]. The ratio of the peak heights of either peaks *a*:*c* or peaks *b*:*c* provide a semi-quantitative identification of the number of P in the polyphosphate chain length [5,7,46]. The FY mode spectrum (~50 nm sensitivity) shows a smaller *a*:*c* ratio relative to the TEY spectrum (figure 1). This indicates that the bulk of the ZDDP antiwear film is composed of shorter-chain polyphosphates than the surface. This has been observed previously [2,7]. Yin *et al.* [46] found that an *a*:*c* height ratio of ~0.3 corresponds to ~8 P and *a*:*c* of ~0.5–~40 P in the polyphosphate chain. The FY spectrum for the bulk ZDDP antiwear film spectrum has a relative peak height ratio of ~0.16, less than the ~0.60 for the TEY spectrum.

The antiwear film formed from ZDDP and the overbased detergent (ZDDPdet) (figure 1 bottom) shows features characteristic of a calcium phosphate. Peak *c* of $Ca_3(PO_4)_2$ is shifted to lower energy by ~0.5 eV compared to the Zn polyphosphate and aligns with that of the ZDDPdet film. The broad shoulder s_1, observed on the high-energy side of peak *c* also aligns well with that of the film. The shoulder s_1 has been observed previously [29] and is due to the incorporation of calcium into the phosphate glass structure but an assignment for this peak has not been made. The calcium incorporation is due to the nature of the overbased detergent which has an excess of $CaCO_3$ used to maintain the alkalinity. The abundance of calcium, in solution, is then easily incorporated into the polyphosphate glass as a network modifier and is thus responsible for creating the shorter-chain structure [11,47]. Peak s_2 at ~142 eV in the ZDDPdet film is due to a second order carbon signal (285 eV/2 = 142 eV) also

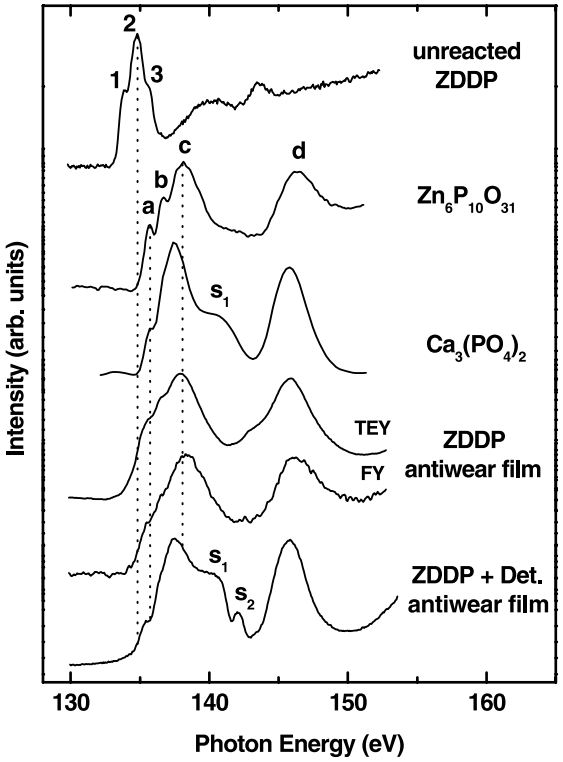

Figure 1. Phosphorus L-edge macroscale XANES spectra of unreacted ZDDP, model polyphosphates, and the antiwear films generated from a ZDDP solution and a ZDDP plus calcium sulphonate (overbased) detergent solution are shown.

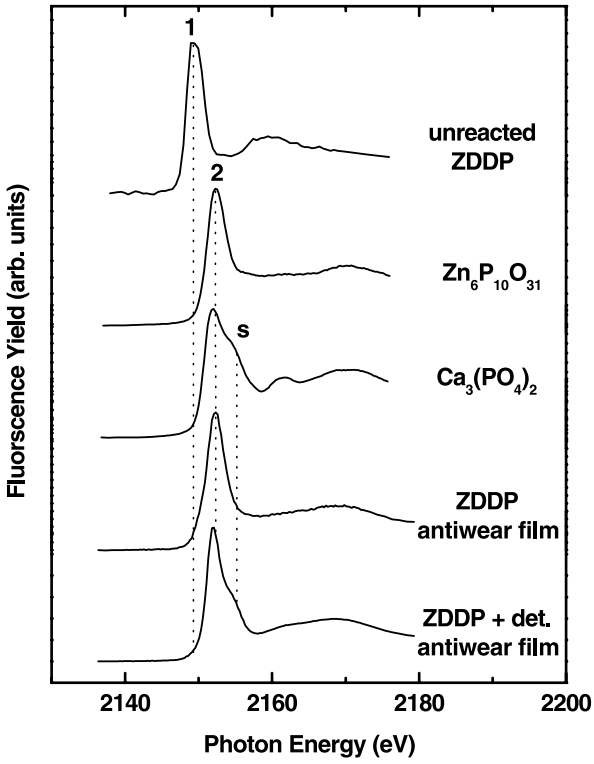

Figure 2. Phosphorus K-edge macroscale XANES spectra of unreacted ZDDP, model polyphosphates, and the antiwear films generated from a ZDDP solution and a ZDDP plus calcium sulphonate (overbased) detergent solution are shown.

indicative of carbon incorporation into the film. The relative peak *a*:*c* height ratio for the macroscale ZDDPdet spectrum is ~0.20. This is less than that measured for the ZDDP antiwear film indicating a shorter-chain polyphosphate structure. As was observed by Kasrai *et al.* [29], our FY spectrum (not shown) was identical (slightly poorer signal-to-noise ratio), having no change in the *a*:*c* peak height ratio indicating that the film is uniform and mostly shorter-chain than the ZDDP antiwear film. It is highly plausible, due to the availability of zinc from ZDDP, that the film formed from the ZDDPdet solution is primarily a shorter-chain calcium polyphosphate glass intermixed with some zinc phosphate. However, the Ca/Zn ratio cannot be obtained from these spectra.

3.2. Macro analysis at the phosphorus K-edge, XANES

Figure 2 shows the fluorescence yield (FY) P K-edge spectra obtained for the ZDDP and the ZDDPdet antiwear film. Also shown in figure 2 are spectra for unreacted ZDDP and $Zn_6P_{10}O_{31}$ polyphosphate and $Ca_3(PO_4)_2$. The P K-edge also provides chemical information about the chemical state of the P species contained in the film. The K-edge measures the transition of core 1s electrons to unoccupied *p*-like valence states. The surface sensitivity is ~50 nm for the TEY mode and >800 nm in the FY mode [32]. Thus the FY spectra shown in figure 2 provide bulk information about the films (the TEY spectra were essentially identical and thus are not shown). It can be observed that the antiwear films spectra have shifted to higher energy compared to that of the unreacted ZDDP. Comparison of the ZDDP antiwear film to the polyphosphate glasses shows that the film is essentially zinc polyphosphate. Lack of a pre-edge peak (low energy side of peak 2) indicates that there is no iron phosphate located in the bulk of the film [29]. A difference between zinc polyphosphate and calcium phosphate can be observed when comparing $Zn_6P_{10}O_{31}$ to $Ca_3(PO_4)_2$. The main peak at ~2152 eV (in $Zn_6P_{10}O_{31}$) is shifted to slightly lower energy (2151.8 eV) in the $Ca_3(PO_4)_2$ orthophosphate, in agreement with the L-edge shift discussed above. Furthermore a shoulder, labelled *s*, at ~2155 eV can be observed which is associated with calcium. Comparison of the ZDDPdet film to the $Ca_3(PO_4)_2$ orthophosphate glass shows the small shift of the main peak 2, to lower energy and the shoulder *s* at ~2155 eV. The shoulder at 2155 eV is due to the incorporation of calcium from the $CaCO_3$ from the overbased detergent, in agreement with the results found in the corresponding L-edge spectra [27, 48]. This has also been reported by infrared studies by Willermet *et al.* [11,47].

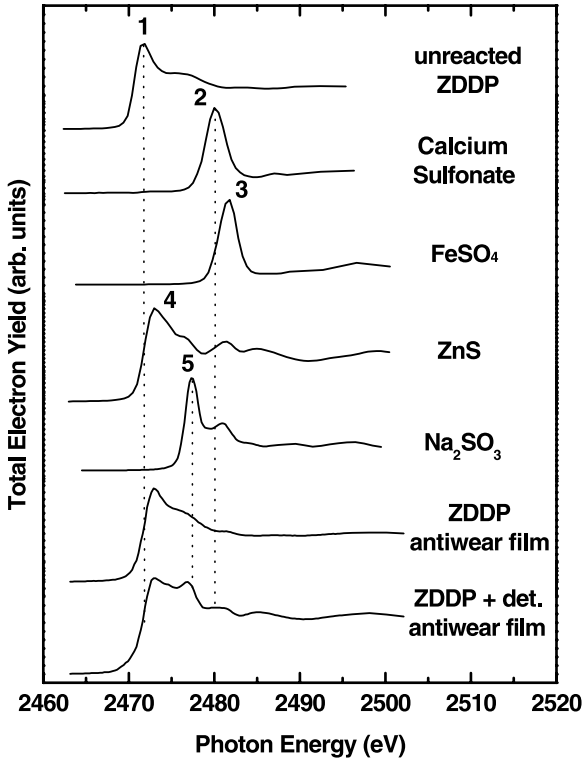

Figure 3. Sulfur K-edge macroscale XANES spectra of unreacted ZDDP, model compounds, and the antiwear films generated from a ZDDP solution and a ZDDP plus calcium sulphonate (overbased) detergent solution are shown.

3.3. Macro analysis at the sulfur K-edge, XANES

The S K-edge macro XANES spectra of model compounds and antiwear films formed from ZDDP alone and in combination with overbased calcium sulfonate (ZDDPdet) are presented in figure 3. It can be observed that a significant portion of the antiwear films is composed of the reduced form of sulfur (-II). It can be noted that the ZDDP antiwear film spectrum is essentially identical to ZnS. On addition of the overbased sulfonate detergent to ZDDP, the resulting antiwear film composition changes somewhat. Although a significant proportion of the film has sulfur in the reduced species, very little calcium sulfonate (peak 2) can be detected. A large peak at ~2477 eV indicates the formation of a sulfite (S^{IV}) observed as peak 5. Kasrai *et al.* [49] describe this process as the disproportionation of sulfonate to form sulfite and some sulfate (S^{VI}, see peak 3) in the bulk (~50 nm) of the film. The small amount of sulfate contained in the film is a reflection of the stability (in air) of the high-overbased detergent [49]. Wan *et al.* [27] also found that addition of calcium phenate to a ZDDP solution resulted in the formation of sulfate and sulfite in the antiwear film. Furthermore, when the amount (wt.% phenate) was increased the amount of sulfite increased, helping to explain the intense peak at ~2477 eV.

3.4. Analysis at the sulfur L-edge, XANES and X-PEEM

The S L-edge macro-TEY spectra for unreacted ZDDP, $FeSO_4$, ZnS and the overbased calcium sulfonate are shown in figure 4. Also shown are the spectra obtained from the ZDDP antiwear film and the ZDDPdet antiwear film, as well as a spectrum extracted from the X-PEEM data for the ZDDPdet film. The S L-edge TEY spectra probe the topmost 5 nm of the surface. Peak *a* is due to the reduced form of sulfur (-II). The characteristic quartet is observed for unreacted ZDDP. Peak *a* is also present in the ZnS spectrum. Peaks *b* and *c* observed for the detergent is due to the sulphonate (S^{V}).

It can be observed that there is a depletion of sulfur at the surface of the ZDDP antiwear film. Peak *a* is very broad and it appears that the sulfur species present is mostly unreacted ZDDP combined with some ZnS character. Broad peaks at ~173 and ~181 eV indicate that some sulfate (S^{VI}) is present at the surface of the film. Peaks 1 and 2 are assigned to the second order (~350 eV/2 = 175 eV) doublet associated with calcium [27,31]. These peaks suggest the presence of calcium on the surface of the film. As was shown above, calcium phosphate is the primary phosphate species in the antiwear film when overbased detergent is mixed with ZDDP. Similar spectra were obtained by Wan *et al.* [27] for a ZDDP plus calcium phenate detergent and by Kasrai *et al.* [48,49] for low and high overbased calcium sulfonate detergents. Examination of the ZDDPdet antiwear film also shows weak peaks *b* and *c*, an indication that some unreacted calcium sulfonate is present in the film.

X-PEEM imaging was also performed at the S L-edge for both films. Sulfur was not detected in the ZDDP antiwear film and trace amounts were detected in the ZDDPdet film (see bottom spectrum in figure 4). There is a small indication of some unreacted ZDDP by the presence of peak *a*. There are two broad peaks also observed at ~173 and 181 eV which indicate that sulfur has been oxidized to sulfate. No second order calcium was detected because of the very low second order component from the 6 m-TGM beamline. Unfortunately no changes in chemistry were detected between different regions in the X-PEEM S L-edge stack for the ZDDPdet film. The smaller area selection used, in the X-PEEM analysis, resulted in much weaker total electron yield spectra and thus a poor signal-to-noise ratio, making it impossible to spatially map the sulfur species in the film.

3.5. X-PEEM: Micro XANES spectroscopy at P L-edge

The microchemistry of the films can now be obtained using X-PEEM spectroscopy at the P L-edge

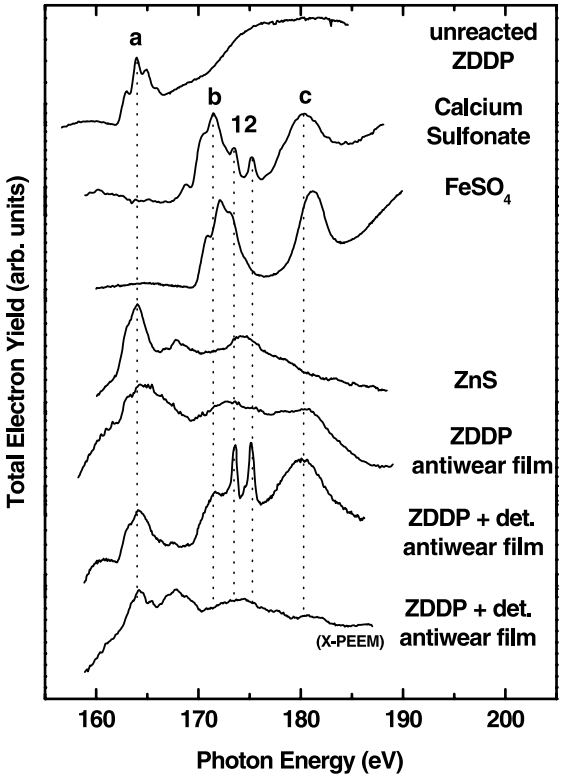

Figure 4. Sulfur L-edge macroscale XANES spectra of unreacted ZDDP, model compounds, and the antiwear films generated from a ZDDP solution and a ZDDP plus calcium sulphonate (overbased) detergent solution are shown. In addition, an X-PEEM spectrum from the ZDDPdet film is also shown.

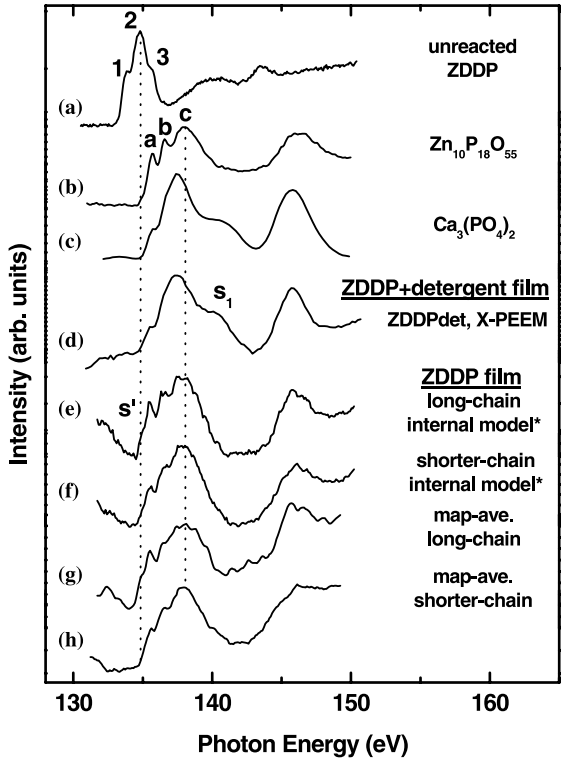

Figure 5. Phosphorus L-edge macroscale XANES spectra of unreacted ZDDP (a) and model polyphosphates (b, c). Also shown are the X-PEEM spectra obtained from selected regions in the antiwear films generated from a ZDDP plus calcium sulphonate (overbased) detergent solution (d) and a ZDDP solution (e–h). *The internal model spectra are identical to those used in reference [7] which is possible since the zoomed region is from the same P L-edge spectromicroscopy stack.

and compared to the macroscale spectra obtained in figure 1. The X-PEEM areas are orders of magnitudes smaller than obtained from the conventional XANES spectra (4 mm^2); typical areas can be several tens of nm^2 to tens of μm^2. In figure 5, X-PEEM spectra (*TEY mode*) obtained from the ZDDPdet antiwear film (spectrum D) and ZDDP antiwear film (spectra E and F), are shown. Comparison of spectrum D to the model calcium phosphate (spectrum C) indicates that the ZDDPdet film spectrum is very similar to that of calcium phosphate. All the features including peak height ratio of peaks a:c, the slight shift to lower energy (of peaks *a–c*) and the presence of shoulder s_1 are very similar. On the other hand, spectra E and F, from the ZDDP film, are remarkably similar to the zinc polyphosphate (spectrum B). Shoulders' is due to the presence of a small amount of unreacted ZDDP and its effect will be discussed later. Comparison of these spectra to the corresponding large area spectra in figure 1 reveals that similar resolution and chemical information can be obtained from the micro-spot of X-PEEM analysis! It is not surprising that the X-PEEM spectra are quite similar since the probing depth of the low energy, secondary electrons collected by the X-ray spectromicroscope is essentially the same as TEY XANES spectra [32,35]. Areas for analysis were selected from within the spectromicroscopy stack, because they were identified as being large or small antiwear pads, located between pads, or had unusually high or low electron intensity in the stack image. The software [36,50] allows for selection of a single pixel, or regions of several pixels in size to extract XANES spectra. The spectra resulting from the selected regions are an average spectrum over all the pixels contained in the region. Thus some spectra are the average of a few pixels (usually have poor signal-to-noise) or several tens to hundreds.

Spectra E and F, of the ZDDP antiwear film, were extracted from the stack and used because they are obviously different and had good signal-to-noise ratios. They also provided well resolved peaks *a*, *b* and *c*, which is due to the small selected areas and therefore less "mixing" of spectra from areas containing unreacted ZDDP, partially reacted ZDDP as well as differing chain lengths of polyphosphate. Furthermore and most importantly, they have different relative peak *a*:*c* height ratios. Spectrum E has a larger *a*:*c* ratio and is thus representative of "longer-chain". It is important to note that the backgrounds are slightly different between these spectra and the macroscale spectra

(in figure 1) and thus only a semi-quantitative comparison of polyphosphate chain length can be made. These spectra are labelled as internal model spectra since they were acquired from within the spectromicroscopy stack. It should be noted that these spectra are identical to those used in Ref. [7] since they are acquired from the same stack-sequence, but from a different region. Spectra G and H are also obtained from the spectromicroscopy stack of the ZDDP antiwear film and their method of extraction will be discussed more thoroughly below.

3.6. Chemomechanical mapping

3.6.1. ZDDP antiwear film

Fiducial marks placed across the wear scar allowed for locating and re-locating of features of interest. These features, generally large antiwear pads, were selected for investigation because they have been suggested as being responsible for limiting asperity contact. Thus, it is beneficial to study these pads thoroughly to understand their chemical identity and mechanical response under pressure. Other areas of interest are found between the large antiwear pads where unreacted or reaction intermediates of ZDDP are thought to be present. AFM topography images allowed for the initial selection of these regions. Spectromicroscopy image sequences (stacks) were taken at these locations at the P L-edge. We have performed similar analysis on ZDDP films in a previous study [7]; however we want to emphasise that the results are reproducible, in different areas of a ZDDP film and use these new results to compare to the ZDDPdet film. Once the correlation between the topography images and the spectromicroscopy stacks were made, areas and selected features were chosen to extract spectra. As was briefly described above, regions that had interesting features such as high or low signal intensity, or had larger pads, small pads, or between antiwear pads were examined. Once spectra, with decent signal to noise ratios, were obtained and had significantly different *a*:*c* peak height ratios, chemical distribution maps could be made.

In figure 5 the internal model spectra for the long- and shorter-chain polyphosphates (spectra E and F) can be observed. Comparison between the two spectra show a significant difference in the relative peak height ratios of peaks *a*:*c* and that both spectra are very similar to the zinc polyphosphate (spectrum B). The internal standard method, which allows for the most accurate mapping when regions of pure material cannot be identified in an area, was used in all cases [23]. A pixel-by-pixel linear regression procedure, using the singular value decomposition (SVD) technique [23], was used to derive the polyphosphate component maps from the internal model spectra. Component maps are images that identify the spatial distribution of chemical species that are similar, for example in this case distinguishing areas of long- and shorter-chain polyphosphates. Once the component maps have been created they are used to generate individual signal masks. A signal mask allows for selection, in an X-PEEM stack, of all pixels with virtually identical spectra. These pixels are averaged to produce long- and shorter-chain map average spectra. In figure 5, spectra G and H show the map average spectra obtained from the spectromicroscopy stack for the long- and shorter-chain regions. It can be observed that, as expected, the spectra have significantly different *a*:*c* peak height ratios and that they are almost identical to the original internal model spectra used (spectra E and F). This is an indication of the success of the mapping procedure. A small shoulder at the low energy side of peak *a*, has been labelled *s*′ and represents some unreacted ZDDP. This was identified in both the long-chain internal model and map average spectra. This indicates that in the regions where long-chain polyphosphates are found, so too is some unreacted ZDDP. This may be one of the beneficial properties of ZDDP as an antiwear agent because as the film wears away there is unreacted ZDDP ready to replenish the antiwear pads at these high contact points. It is important to note that this small peak will have a small effect on the relative peak height of peak *a* however the difference in the relative peak heights between the long- and shorter-chain polyphosphates are still significant enough to distinguish a difference. The component maps are then used to create a polyphosphate distribution map.

Figure 6 shows secondary electron X-PEEM images (a and c) of a large, elongated antiwear pad, along with the respective polyphosphate distribution maps (b and d). An AFM topography image of this antiwear pad can be seen in figure 7 for comparative purposes. Figure 6(c) and (d) shows the effect that the 10 Å platinum coating has on the charging of the thick polyphosphate film. In figure 6(a) dark patches can be observed along the antiwear pad. These are charging regions where electron emission has been suppressed due to the non-conducting nature of the polyphosphate, particularly where the film is thick. This pad is known to be thick by measurements made with the AFM (figure 7(c)). Even with charging, quality spectra could still be obtained from selected regions and were found to have significantly different *a*:*c* relative peak height ratios (see spectra in figure 5). It was also possible to map the polyphosphate distribution in the antiwear film. Yellow symbolises longer-chain (*a*:*c* $\sim$0.74) and blue represents shorter-chain (*a*:*c* $\sim$0.52) polyphosphates. However, when the platinum coating was sputtered onto the polyphosphate film an electrical contact was made around the pads and the number of electrons at each pixel increased, with the large pads giving the brightest regions (see figure 6(c)) rather than the darkest in the uncoated sample (figure 6(a)). This eliminated the charging and decreased the residuals

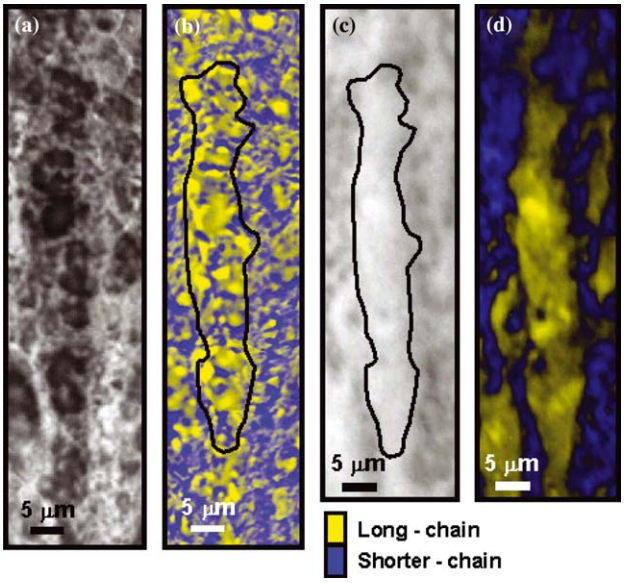

Figure 6. The secondary electron images obtained by the X-PEEM (a and c) and the corresponding polyphosphate distribution map (b and d). Figures (a) and (b) are from the non-coated sample and Figures (c) and (d) are from the sample after it was sputter coated with 10 angstroms of platinum. The large antiwear pad of interest is outlined. A difference in the quality of mapping can be observed after the platinum sputter-coating is applied. Yellow in the polyphosphate distribution map indicates the location of longer-chain polyphosphates and blue represents the location of shorter-chain polyphosphates. A colored version of this figure can be found in the PDF version of this document.

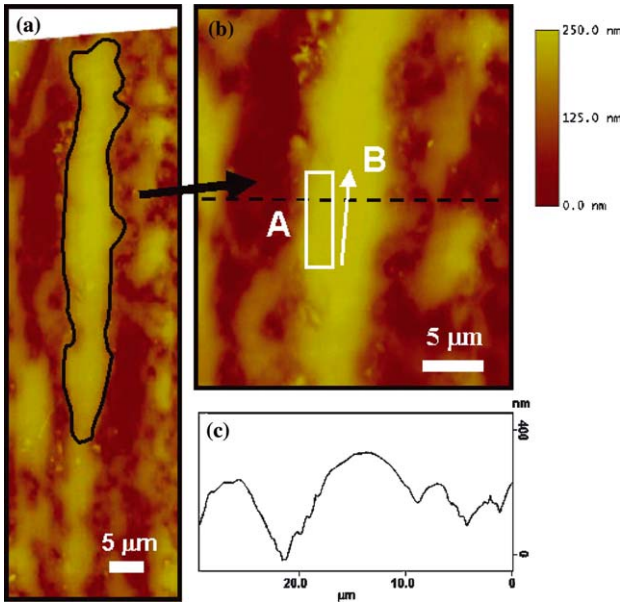

Figure 7. An AFM topography image of the elongated antiwear pad in figure 6. The large antiwear pad of interest is outlined in (a). A zoomed region of (a) is shown in (b). Region A and Path B are marked to show the locations where nanoindentation measurements were performed. A topographic profile image taken along the dotted line in (b) is shown in (c). A colored version of this figure can be found in the PDF version of this document.

from the fitting procedure, clearly making a better polyphosphate distribution map (figure 6(d)). A difference was detected in the relative peak height ratios of peaks *a*:*c* of the spectra obtained, when the film was coated. However, the *a*:*c* difference was large enough to still distinguish large and shorter-chain polyphosphates. As can be seen by comparing figure 6(b)–(d), the general trend is still preserved. More detail about the charging and the effect of the coating on the spectroscopy of the polyphosphate film will be discussed in a forthcoming publication.

Figure 7(a) and (b) are the corresponding AFM topography images that allow for an accurate examination of the morphology and height of the elongated antiwear pad. It can be observed in figure 6(d) that a significant portion of the elongated antiwear pad has long-chain polyphosphates at the surface. Also from the topography image it can be seen that the lower regions (darker areas) are made up primarily of shorter-chain polyphosphates in figure 6(b) and (d). Figure 7(b) shows an enlargement of the center portion of the elongated antiwear pad. This topography image allows for accurate determination of the height profile of the antiwear pad. A cross-sectional analysis of the pad was performed along the dotted line in figure 7(b). The sectional analysis is shown in figure 7(c). From this figure the antiwear pad can be found to be ~300 nm thick.

A series of nanoindentations were performed in Region A at the edge of a large pad outlined by the box and along the Path labelled B in the middle of a pad. Indents were performed to maximum loads of 50 μN, to measure accurately the mechanical properties of the film without sensing the steel substrate below the film. This load generally had maximum penetration depths of <15 nm which does not exceed the 10% rule-of-thumb for measuring the mechanical properties of soft materials on hard substrates [40,42,43]. The indention modulus (E_s^*) was calculated using the technique suggested by Oliver and Pharr [39] and utilises the initial slope of the unloading curve. The f–d curves representative of the two areas (A and B) and one taken in 52100 steel (no film) are shown in figure 8. The calculated indentation modulus (E_s^*) for Region A was determined to be 87.8 ± 3.9 GPa from f–d curves taken at the edge of the pad and that for f–d curves taken along Path B, to be 119.5 ± 5.8 GPa. Typical values obtained for steel range between 210 and 250 GPa. The values in parenthesis beside the values listed in figure 8 are the number of E_s^* values, calculated from f–d curves, averaged together to determine the value. The statistical errors given for these averages represent a standard deviation of 2σ and are quite small. This indicates that these values are statistically quite different for the edge and the middle of the antiwear pad in this region. Values similar to these, obtained for the ZDDP antiwear film, by others

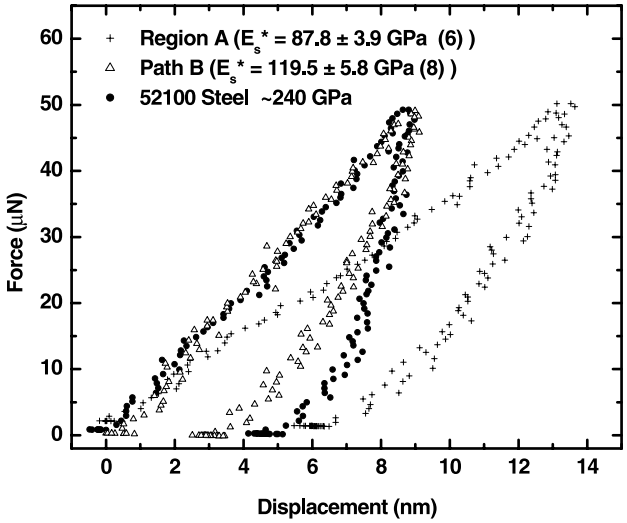

Figure 8. Representative force-distance curves for Region A and along Path B as indicated in figure 7(b).The average reduced elastic moduli E_s* values calculated from the f–d curves are also given. The values in parenthesis indicate the number of values used to calculate the average and statistical error.

[12–14,16,17] are on average, between 70 and 120 GPa. The measure of the stiffness of a material can be determined by the slope of the initial portion of the unloading curve, the stiffer the material the steeper the slope. It can be observed that 52100 steel has the steepest unloading curve followed by Path B and then Region A. The maximum depth of penetration into the film is defined as the total displacement into the film at maximum load. For the representative indent on Path B and into the 52100 steel, this is ~9 nm. This indicates that we are only measuring the near-surface region of the antiwear pad. This is very close to the sampling depth of the TEY signal obtained from the X-PEEM (2–5 nm). These values indicate that the center of the antiwear pads is stiffer than the edges. It is important to point out that the f–d curves were taken >300 nm apart to avoid influence from neighbouring indents. Furthermore, the indentation experiments taken along the edge of the antiwear pad was significantly far (>500 nm) from the edge of the antiwear pad as to avoid irregularities in the response of the film. The shape of the f–d curve can also tell a lot about the material response. Hysteresis between the loading and unloading portions of the f–d curve indicates the elastic behaviour of the film. Force curves with no hysteresis indicate that the film has fully recovered after unloading and is thus elastic. It can be observed from these f–d curves that the center of the pad (Path B) has a greater elastic response than the edge (Region A); the hysteresis in the curve representative of Region A is larger (~8 nm compared to 4 nm). Furthermore, it can be observed that the center of the pad has a larger recovery in the hysteresis than steel indicating that it is also more elastic than steel. Others using an IFM [12] observed this trend. However, Graham *et al.* [12] found a larger variation between the center and edge of the pad. This may be due to the difference in calculation of indentation modulus and also the geometry of the indenter tip. In this study, with a Berkovich diamond tip (radius: 100–160 nm), the E* measured averages the material response over a larger area than that measured using the smaller (<80 nm) IFM tip. This may also be an indication of the heterogeneity of the film suggesting that comparing exact numbers between researchers has to be done with caution.

A second area of the same antiwear film was chosen for analysis. This region is located in an area composed of smaller antiwear pads, with lower height profiles between large elongated pads. Figure 9(a) shows the X-PEEM electron image of the antiwear pad. The dark region in the center of the image is the antiwear pad; the antiwear pad is sufficiently thick that it charges in the secondary electron image, resulting in electron suppression and a dark hue in the image. An image was acquired after the film was sputter coated with platinum, which eliminated the charging and is not shown. The polyphosphate distribution map, generated from the internal model spectra shown in figure 5 is shown for this region in figure 9(b). The use of the same internal model spectra was possible since both these regions were located on the same full-scale X-PEEM spectromicroscopy stack. Figure 9(c) shows the AFM topography image of the region of the antiwear film examined. The area surrounded by the white box is the antiwear pad highlighted in images A and B. In the polyphosphate distribution image, it can be seen that the antiwear pad has a larger distribution of the longer-chain polyphosphates (yellow regions). This region also shows that the adjacent areas also contain a significant amount of long-chain polyphosphates. This may be another positive feature of ZDDP antiwear film formation, in that longer-chain polyphosphates form quite quickly even in lower lying regions of the antiwear film. As was found in other areas of the ZDDP film using X-PEEM [7], intermixing of long-, shorter-chain and unreacted ZDDP was found in-between and around the large antiwear pads. This may be ideal under rubbing conditions where these regions act like reservoirs able to replenish the film as it wears away.

3.6.2. ZDDP + detergent antiwear film

The morphology of an antiwear film formed from a solution containing 1.2 wt.% ZDDP and 2 wt.% calcium detergent is significantly different than from a solution of 1.2 wt.% ZDDP alone. In figure 10, AFM topography images show characteristic regions of the respective antiwear films (sliding direction is horizontal across both films). Figure 10(a) is that of the ZDDP antiwear film and figure 10(b) for the ZDDPdet film (both have the same height scales). The *good* antiwear

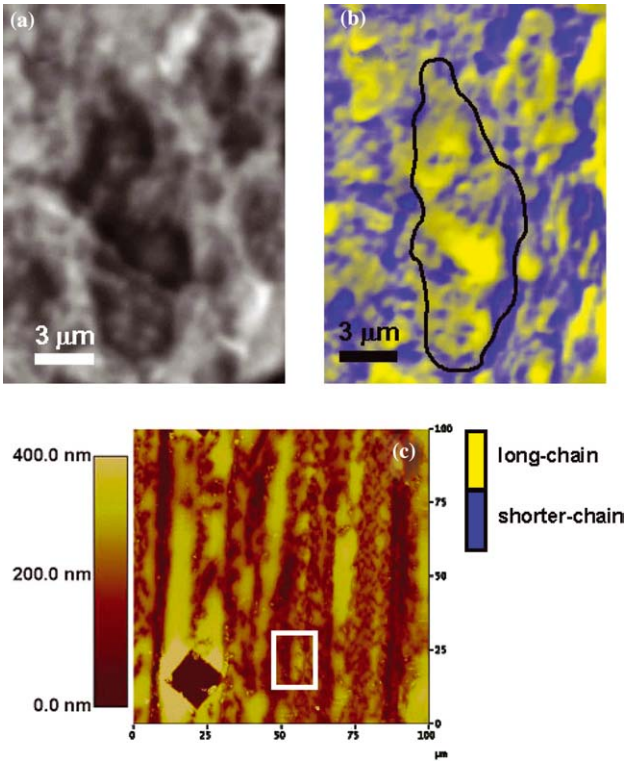

Figure 9. The secondary electron image obtained by the X-PEEM (a) and the corresponding polyphosphate distribution map (b) are shown for a different ZDDP antiwear pad. An AFM topography image (c) shows the location of the antiwear pad in (a) and (b) outlined by the white box. Yellow in the polyphosphate distribution map indicates the location of longer-chain polyphosphates and blue represents the location of shorter-chain polyphosphates. A colored version of this figure can be found in the PDF version of this document.

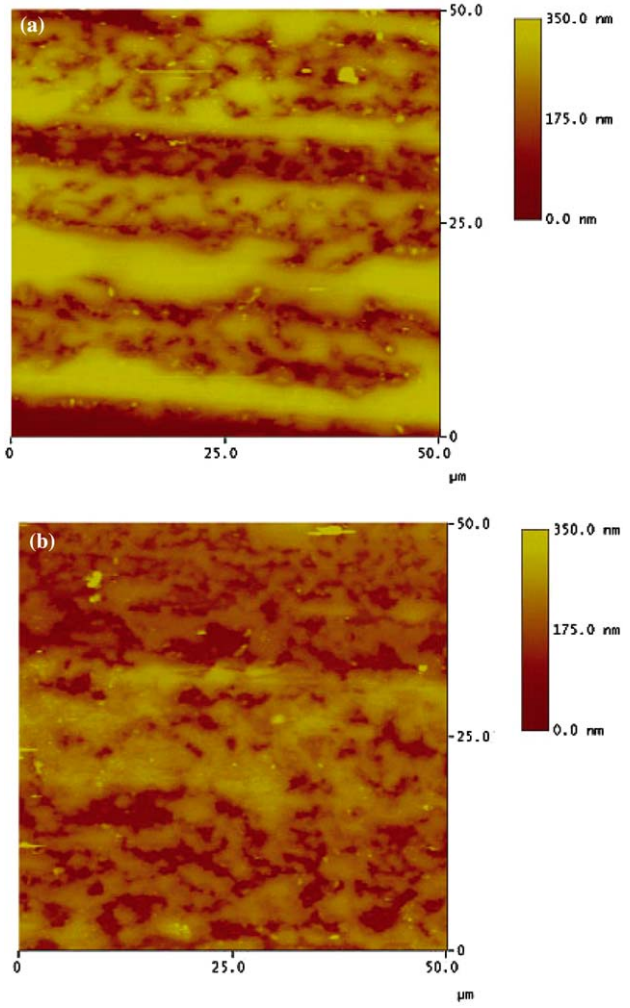

Figure 10. AFM topography images of the ZDDP antiwear film (a) and ZDDPdet antiwear film (b) show differences in the morphology of the films. Differences in the sizes of the antiwear pads and height profiles can be observed. Identical scale bars are provided. A colored version of this figure can be found in the PDF version of this document.

film is obtained by ZDDP alone and has significantly larger antiwear pads that are elongated in the direction of rubbing. The antiwear pads (or streaks) are several tens of microns long and several microns wide. Furthermore the film's thickness is greater than 250 nm in many locations. The ZDDPdet antiwear film has a much smaller thickness never exceeding 200 nm; in fact, greater than 60% of the film lies below this threshold. In contrast, it appears that $>50\%$ of the ZDDP antiwear film is above 250 nm. Furthermore, the film appears flat and the antiwear pads do not have the convex morphology that they do in the ZDDP film. This film is similar in morphology to an aryl-ZDDP film generated under the same conditions [13] but with no detergent, which was also found to have poor antiwear characteristics. It appears that the addition of the detergent is in some way affecting the mechanism by which the film forms and sustains itself.

An AFM topography image is shown in figure 11(a) from the ZDDPdet film. *Larger* antiwear pads and smaller smeared regions can be observed. It should be noted that these *larger* antiwear pads are still significantly smaller than the large antiwear pads found in the antiwear film formed from a solution containing only ZDDP. Analysis of the selected areas, shown in figure 11(b) gave spectra as shown in figure 11(c). Several regions of the film were examined using X-PEEM. An image was acquired after the film was sputter coated with platinum, which eliminated the charging and is not shown since the antiwear pads are easily seen in the charging image. Many regions were selected for spectra extraction. These areas consisted of low or higher intensity electron signal in the electron images; and were recorded on large or small antiwear pads, or on regions between or around antiwear pads. The spectra for the selected regions are numbered corresponding to the numbers in the X-PEEM image. Others are not shown since most were identical. The spectra are an average of the spectra from all pixels contained in each of the outline areas. All spectra

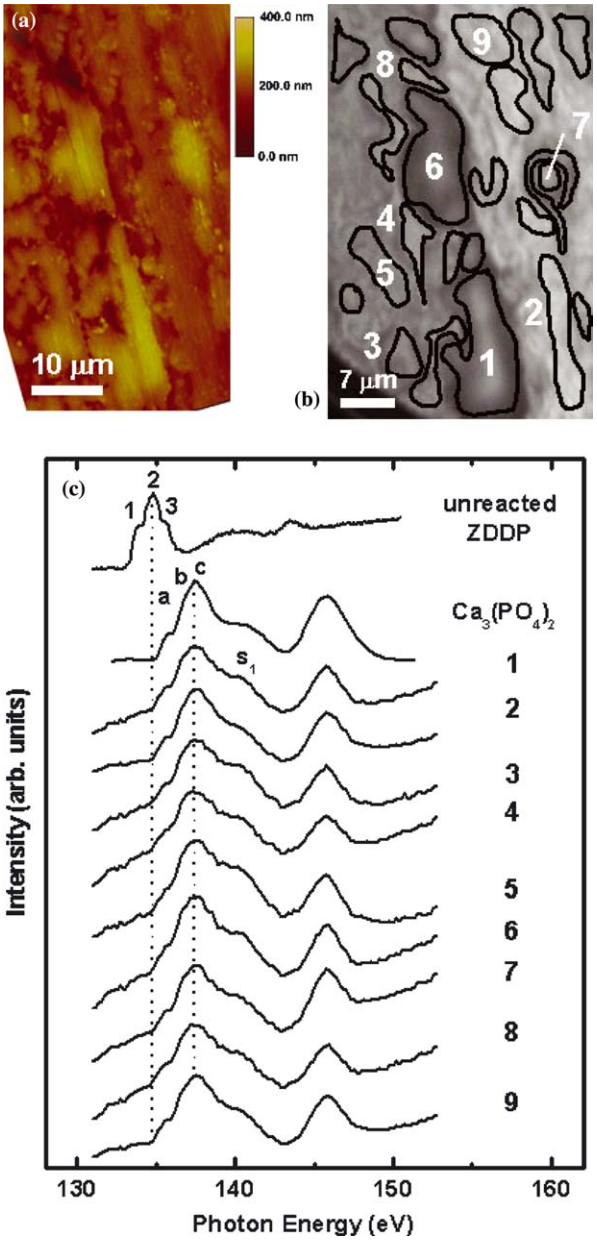

Figure 11. An AFM topography image of the ZDDPdet film (a) shows smaller antiwear pads. An X-PEEM image of the corresponding region shows the areas that were selected to extract P L-edge XANES spectra using the X-PEEM software. Some regions are numbered to identify the corresponding spectra in (c). In most cases the film was chemically identical and so only a selected few regions are shown. A colored version of this figure can be found in the PDF version of this document.

appear identical. The average relative peak height ratios for peaks *a*:*c* is ~0.35–0.40. This is in contrast to what was found for the ZDDP antiwear film (>0.50 see figures 1 and 5 for example). From figure 11(c), it can be determined that the film has a calcium orthophosphate structure. The shoulder marked s_1 is an indication of the calcium contained in the film. Furthermore there is a slight shift to lower energy of peak *c*, which is characteristic of calcium phosphate glasses (see figure 1 for example). One small difference that can be observed in the spectra is the height of the shoulder s_1. In some spectra, this is higher than in others. It has been suggested that the intensity of this shoulder is an indication of the amount of calcium in the film [27]. Since the phosphate spectra were similar in all regions, it was not possible to create polyphosphate distribution maps.

Understanding the mechanical response of ZDDP antiwear films is beneficial to determining how it responds under load. It has previously been determined that in the ZDDP antiwear film, the large antiwear pads, have longer-chain zinc polyphosphates at the surface and shorter-chain polyphosphates in the bulk [2, 7]. New insight into the mechanical response of antiwear films could be provided if a difference in modulus can be measured for the film, when the surface and the bulk of the film is identical. This would help to determine exactly what characteristics are ideal for preventing wear. Since the ZDDPdet antiwear film is composed entirely of shorter-chain polyphosphates and has an anti-synergistic effect on wear, it is highly plausible that the film may have a different mechanical response than when it has a layered structure. Detailed nanoscale mechanical characterization of the ZDDPdet antiwear film is shown in figure 12. Since the film was found to be thinner than the ZDDP antiwear film, maximum applied loads for the indentation experiments were kept low (35 μN). This resulted in average penetration depth of <11 nm into the film. Several indents were taken on selected features. Each indent was spaced ~500 nm from its neighbours. The average indentation modulus for each of three antiwear pads is shown in figure 12. Figure 12(a) shows an AFM topography image with the antiwear pads (with markers) that were mechanically tested by nanoindentation. Representative f–d curves are shown in figure 12(b) for each of the three pads. These are compared to an f–d curve taken into steel to the same maximum load. It can be observed that the films all have relatively similar elastic responses to the indentation procedure (within statistical error). The average extracted E_s^* values are shown for each antiwear pad (the number in parentheses is the number of f–d curves taken in each pad; the E_s^* is calculated for each f-d and averaged together to give the average E_s^*). The large number of f–d curves taken, resulting in a small statistical error, signifies a good consistency in the calculated E_s^* for each antiwear pad. The E_s^* values varied between 83 and 90 GPa. Furthermore this is an indication that the antiwear pads formed from the ZDDPdet film are more homogeneous than those formed from the ZDDP alone solution. These values are statistically different from the values obtained earlier for the ZDDP antiwear film 119 GPa for the center and 90 GPa for the edges. These results indicate that there is in fact a difference in mechanical properties between

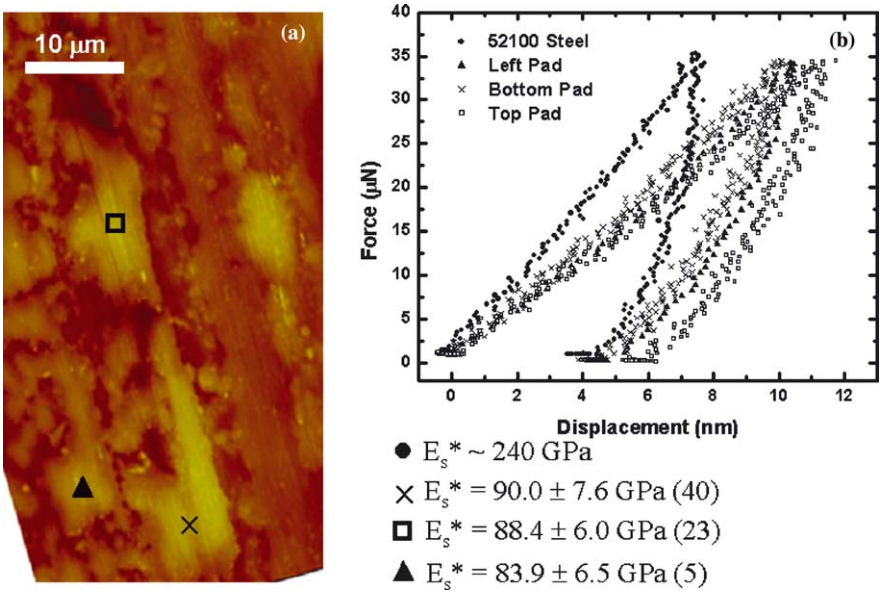

Figure 12. An AFM topography image of the ZDDPdet film (a) shows smaller antiwear pads that are marked corresponding to the indentation analysis. Representative force-distance curves for the corresponding antiwear pads are shown (b). Also listed are the average indentation moduli and statistical error calculated from the number of f–d curves listed in the parenthesis. A colored version of this figure can be found in the PDF version of this document.

the antiwear pads in a ZDDP antiwear film to a ZDDPdet antiwear film. This is the first time that the nanoscale mechanical properties of an antiwear film formed from a solution containing ZDDP and a detergent has been measured. Furthermore this is the first time that chemomechanical mapping of a film formed for a solution containing ZDDP plus detergent has been performed.

There are two possible effects that may influence the mechanical response of the ZDDPdet polyphosphate film. The simplest and most probable, theory is that there is an influence due to the $CaCO_3$ which has been incorporated into the film. Analysis of the C K-edge of the detergent film showed the presence of calcium carbonate (not shown). Giasson *et al.* [51,52] using infrared reflection absorption spectroscopy, found that rubbing of overbased calcium sulfonate alone in base oil resulted in the formation of a film containing calcium carbonate which can crystallize to form calcite. Willermet *et al.* [11,47] found carbonate in the film when ZDDP was added to the base oil. Wan *et al.* [27] using C K-edge XANES found that calcium carbonate was in the film and that the result of increasing the total base number (hence the amount of $CaCO_3$) resulted in a film that had a lower phosphorus areal content per mass area. These findings are all in agreement with our P and S K- and L-edge results.

The second explanation may be centred on the probing depth of the indentation experiments and that for the X-PEEM measurements. X-PEEM analysis is performed on the top 2–5 nm of the surface. Indentation experiments probe the top 10–20 nm of the film. It is possible that in the ZDDP film, which has a layered structure, a majority of the mechanical response of the film is due to the bulk of the film (which is shorter-chain polyphosphate) and not due to the top 2–5 nm of the film. The E_s^* values obtained in this study were measured using a diamond indenter and calculated using the method of Oliver and Pharr [39]. This method calculates the reduced modulus (E^*) of the film based on the slope of the initial portion of the unloading curve. As can be seen from the f–d curves in figures 8 and 12, this is already >10 nm into the film. Thus, the elastic response of the film is dominated by the bulk properties (or short-chain polyphosphate). This may be a reason for the similarity between the edges of the large antiwear pads (from the ZDDP alone film) and the pads in the ZDDPdet film. Measurements of the mechanical properties of the film have previously been performed using an IFM [12–14]. The IFM has the ability to measure the elastic response of the topmost few nanometers of a surface [18–20]. The f–d curves are fitted using Hertzian mechanics that determine the E^* value based on fitting of the initial portion of the loading curve. In many cases this can be only the very first few nanometers of the film penetration. Simply, the steeper the slope, of the initial portion of the loading curve, the stiffer the material. Indentation modulus values obtained for a ZDDP antiwear film, using the IFM, have found values that vary as close to that for steel. This may suggest that the mechanical response of the surface of the ZDDP antiwear pad may be quite different (stiffer) than that for the bulk, which has been measured here. This extrapolation then suggests that the ZDDP antiwear pads have a stiffer elastic shell

than the bulk, which has been suggested earlier [13]. Warren *et al.* [13] found an inflection point in the f–d curves taken on ZDDP that indicated that the tip penetrated a stiffer layer and then entered a softer more compliant layer. They described this event as a plastic threshold.

4. Conclusion

We have provided the first thorough chemomechanical comparison of antiwear films formed from solutions containing ZDDP and ZDDPdet. This has been performed using XANES, X-PEEM and imaging nanoindentation techniques. Using a grid of fiducial marks the same areas, of the antiwear films, were located with all techniques. It was found that:

- AFM images showed that the ZDDP film had a significantly different morphology than the ZDDPdet film. The overall height profile and size of antiwear pads, was larger than that for the ZDDPdet film.
- P L-edge micro-spectroscopy obtained using X-PEEM agreed with that taken on the macroscale, which shows that longer-chain zinc polyphosphates are found at the surface of the film.
- Polyphosphate species were spatially resolved in the ZDDP film. Longer-chain zinc polyphosphates were located at the surface of the large antiwear pads and regions between the pads had predominately shorter-(with some intermixing) chain-length zinc polyphosphates.
- Locations where there were longer-chain polyphosphates also had some unreacted ZDDP.
- X-PEEM showed that the polyphosphate chemistry of ZDDPdet film was uniform on the microscale agreeing with that found from macroscale spectroscopy; both showing shorter-chain calcium phosphate.
- The large, elongated antiwear pads of the ZDDP film were found to have an indentation modulus of $\sim$120 GPa at the center on the pad and $\sim$90 GPa at the edges.
- The large antiwear pads found on the ZDDPdet film had an indentation modulus of $\sim$90 GPa, statistically different than that measured for the center of the pads in ZDDP antiwear film.

The spatial chemistry has thus been evaluated on the same length scale as the mechanical properties providing a chemomechanical map of the antiwear pads. This sheds new insight into the structure and mechanical response of ZDDP antiwear films. Future work using alternate indentation techniques at elevated temperatures, such as that employed by an environmental controlled-IFM (EC-IFM), can help to explore conditions that are more relevant to engine operation and their effect on the mechanical response of the film.

Acknowledgments

M.A.N would like to personally thank A.P. Hitchcock for his help with aXis2000 and useful discussions about the analysis of the X-PEEM data. The authors would also like to thank K. Tan, A. Jurgensen and the staff of the Synchrotron Radiation Centre (SRC), University of Wisconsin, Madison, WI for their technical support. We are grateful to the National Science Foundation for supporting the SRC under award no DMR-00-84402. Financial support was provided by General Motors of Canada Ltd. and Natural Sciences and Engineering Research Council of Canada.

References

[1] I.M. Hutchings, Tribology: Friction and Wear of Engineering Materials (CRC Press, London, 1992).
[2] Z. Yin, M. Kasrai, M. Fuller, G.M. Bancroft, K. Fyfe and K.H. Tan, Wear 202 (1997) 172.
[3] M. Fuller, Z. Yin, M. Kasrai, G.M. Bancroft, K. Fyfe and K.H. Tan, in: Proceedings of International Tribology Conference, Yokohama, 1995, Vol. 2, (Japanese Society of Tribology, Tokyo, 1996) 1113.
[4] Z. Yin, M. Kasrai, G.M. Bancroft, K.F. Laycock and K.H. Tan, Trib. Int. 26 (1993) 383.
[5] M. Kasrai, M. Fuller, M. Scaini, Z. Yin, R.W. Brunner, G.M. Bancroft, M.E. Fleet, K. Fyfe and K.H. Tan, in: Lubricants and Lubrication: Lubrication at the Frontier, Vol. 30, eds. D. Dowson et al. (Elsevier Science B.V., Amsterdam, 1995) 659.
[6] G.M. Bancroft, M. Kasrai, M. Fuller, Z. Yin, K. Fyfe and K.H. Tan, Trib. Lett. 3 (1997) 47.
[7] M.A. Nicholls, P.R. Norton, G.M. Bancroft, M. Kasrai and T. Do, Trib. Lett. 17 (2004) 205.
[8] J.S. Sheasby, T.A. Caughlin and W.A. Mackwood, Wear 196 (1996) 100.
[9] J.S. Sheasby, T.A. Caughlin and W.A. Mackwood, Wear 201 (1996) 209.
[10] Y.Y. Yang, Y.S. Jin and T. Yan, Wear 210 (1997) 136.
[11] P.A. Willermet, R.O. Carter, P.J. Schmitz, M. Everson, D.J. Scholl and W.H. Weber, Lub. Sci. 9–4 (1997) 325.
[12] J.F. Graham, C. McCague and P.R. Norton, Trib. Lett. 6 (1999) 149.
[13] O.L. Warren, J.F. Graham, P.R. Norton, J.E. Houston and T.A. Michalske, Trib. Lett. 4 (1998) 189.
[14] M.A. Nicholls, T. Do, P.R. Norton, G.M. Bancroft, M. Kasrai, T.W. Capehart, Y.-T. Cheng and T. Perry, Trib. Lett. 15 (2003) 241.
[15] A.J. Pidduck and G.C. Smith, Wear 212 (1997) 254.
[16] S. Bec and A. Tonck, in: Tribology Series: Lubricants and Lubrication, Vol. 30, eds. D. Dowson, C. Taylor, T. Childs and G. Dalmaz (Elsevier, Amsterdam, 1996) 173.
[17] M. Aktary, M.T. McDermott and G.A. McAlpine, Trib. Lett. 12 (2002) 155.
[18] J.D. Kiely, K.F. Jarausch, J.E. Houston and P.E. Russell, J. Mater. Res. 14 (1999) 2219.
[19] K.F. Jarausch, J.D. Kiely, J.E. Houston and P.E. Russell, J. Mater. Res. 15 (2000) 1693.
[20] S.A. Joyce, R.C. Thomas, J.E. Houston, T.A. Michalske and R.M. Crooks, Phys. Rev. Lett. 68 (1992) 2790.
[21] C. Jacobsen, S. Wirick, G. Flynn and C. Zimba, J. Microscopy 197 (2000) 173.
[22] C. Morin, H. Ikeura-Sekiguchi, T. Tyliszczak, R. Cornelius, J.L. Brash, A.P. Hitchcock, A. Scholl, F. Nolting, G. Appel,

D.A. Winesett, K. Kaznacheyev and H. Ade, J. Elect. Spectro. Rel. Phen. 121 (2001) 203.
[23] I.N. Koprinarov, A.P. Hitchcock, C.T. McCrory and R.F. Childs, J. Phys. Chem. B 106 (2002) 5358.
[24] G.W. Canning, M.L. Fuller, G.M. Bancroft, M. Kasrai, J.N. Cutler, G. De Stasio and B Gilbert, Trib. Lett. 6 (1999) 159.
[25] C.C. Colyer and W.C. Gergel, in: Chemistry and Technology of Lubricants, Vol. 1, eds. RM. Mortier and S.T. Orszulik (VCH Publishers, Inc., New York, 1992) 62.
[26] Y.Yamada, J. Igarashi and K. Inoue, Lub. Eng. 48 (1992) 511.
[27] Y. Wan, M.L. Suominen Fuller, M. Kasrai, G.M. Bancroft, K. Fyfe, J.R. Torkelson, Y.F. Hu and K.H. Tan, in: Boundary and Mixed Lubrication: Science and Applications, Vol. 40, eds. D. Dowson (Elsevier Science B. V., 2002) 155.
[28] E.S. Yamaguchi, S.H. Roby, M.M. Francisco, S.G. Ruelas and D. Godfrey, Trib. Trans. 45 (2002) 425.
[29] M. Kasrai, M. Vasiga, M.S. Fuller G.M. Bancroft and K. Fyfe, J. Synchro. Rad. 6 (1999) 719.
[30] P. Kapsa, J.M. Martin, C. Blanc and J.M. Georges, J. Lub. Technol. 103 (1981) 486.
[31] Z. Yin, M. Kasrai, M. Fuller, G.M. Bancroft, K. Fyfe, M.L. Colaianni and K.H. Tan, Wear 202 (1997) 192.
[32] M. Kasrai, W.N. Lennard, R.W. Brunner, G.M. Bancroft, J.A. Bardwell and K.H. Tan, Appl. Surf. Sci. 99 (1996) 303.
[33] M. Kasrai, Z. Yin, G.M. Bancroft and K. Tan, J. Vac. Sci. Technol. A 11 (1993) 2694.
[34] B.H. Frazer, M. Girasole, L.M. Wiese, T. Franz and G. De Stasio, Ultramicroscopy 99 (2004) 87.
[35] B.H. Frazer, B. Gilbert, B.R. Sonderegger and G. De Stasio, Surf. Sci. 537 (2003) 161.
[36] A.P. Hitchcock, P. Hitchcock, C. Jacobsen, C. Zimba, B. Loo E. Rotenberg, J. Denlinger and R. Kneedler, aXis2000—program available from http://unicorn.mcmaster.ca/aXis2000.html (1997).
[37] B. Gilbert, R. Andres, P. Perfetti, G. Margaritondo, G. Rempfer and G. De Stasio, Ultramicroscopy 83 (2000) 129.
[38] G. De Stasio, B.H. Frazer, B. Gilbert, K.L. Richter and J.W. Valley, Ultramicroscopy 98 (2003) 57.
[39] W.C. Oliver and G.M. Pharr, J. Mater. Res. 7 (1992) 1564.
[40] A.V. Kulkarni and B. Bhushan, Mat. Lett. 29 (1996) 221.
[41] J. Malzbender and G. de With, Sur. Coat. Technol. 135 (2000) 60.
[42] T. Chudoba, N. Schawarzer and F. Richter, Sur. Coat. Technol. 127 (2000) 9.
[43] G.M. Pharr and W.C. Oliver, MRS Bull. 17 (1992) 28.
[44] M. Fuller, Z. Yin, M. Kasrai, G.M. Bancroft, E.S. Yamaguchi, P.R. Ryason, P.A. Willermet and K.H. Tan, Trib. Int. 30 (1997) 305.
[45] D.G.J. Sutherland, M. Kasrai, G.M. Bancroft, Z.F. Liu and K.H. Tan, Phys. Rev. B 48 (1993) 14989.
[46] Z. Yin, M. Kasrai, G.M. Bancroft, K.H. Tan and X. Feng, Phys. Rev. B 51 (1995) 742.
[47] P.A. Willermet, D.P. Dailey, R.O. Carter III, P.J. Schmitz, W. Zhu, J.C. Bell and D. Park, Trib. Int. 28 (1995) 163.
[48] M. Kasrai, M. Suominen Fuller, G.M. Bancroft, E.S. Yamaguchi and P.R. Ryason, Trib. Trans. 46 (2003) 534.
[49] M. Kasrai, M. Suominen Fuller, G.M. Bancroft, E.S. Yamaguchi and P.R. Ryason, Trib. Trans. 46 (2003) 543.
[50] L.M. Croll, J.F. Britten, C. Morin, A.P. Hitchcock and H.D.H. Stoever, J. Synchro. Rad. 10 (2003) 265.
[51] S. Giasson, T. Palermo, T. Buffeteau, B. Desbat and J.M. Turlet, Thin Solid Films 252 (1994) 111.
[52] T. Palermo, S. Giasson, T. Buffeteau, B. Desbat and J.M. Turlet, Lubr. Sci. 8 (1996) 119.